

# Microstructural evolution and its influence on the superconductivity induced by oxygen vacancies in $\text{Sr}_2\text{VO}_{3-\delta}\text{FeAs}$ ( $\delta = 0.1, 0.5$ )

R. C. Che,<sup>1,\*</sup> F. Han,<sup>2,3</sup> C. Y. Liang,<sup>1</sup> X. B. Zhao,<sup>1</sup> and H. H. Wen<sup>2,3</sup><sup>1</sup>*Department of Material Science and Laboratory of Advanced Materials, Fudan University, Shanghai, 200438, China*<sup>2</sup>*National Laboratory for Superconductivity, Institute of Physics and Beijing National Laboratory for Condensed Matter Physics, Chinese Academy of Sciences, P.O. 603, Beijing, 100190, China*<sup>3</sup>*National Laboratory of Solid State Microstructures, Department of Physics, Center for Superconducting Physics and Materials, Nanjing University, 210093, China*

(Received 27 July 2014; published 9 September 2014)

Superconducting transition temperatures of  $\text{Sr}_2\text{VO}_{3-\delta}\text{FeAs}$  ( $\delta = 0.1, 0.5$ ) can be tuned by adjusting the dopant concentration of oxygen vacancy. The association between microstructure and superconductivity is not clear and urgently needs to be clarified. Directly via the *in situ* transmission electron microscopy (TEM) cooling experiment, we demonstrate novel atomic-level microstructural features, which are induced by oxygen deficiency and play key roles in determining the superconducting property. The poor superconducting sample  $\text{Sr}_2\text{VO}_{2.5}\text{FeAs}$  exhibits high density of stacking faults distributed along the [001] orientation with periodic weak image contrast and extra streaking diffraction spots, due to the periodic extraction of partial SrO atom stripes from the  $\text{Sr}_2\text{VO}_{2.5}$  blocking unit. The superconducting sample  $\text{Sr}_2\text{VO}_{2.9}\text{FeAs}$  shows a well-formed structure with only a limited amount of point vacancies. When  $\delta$  is changed from 0.1 to 0.5, the valence state of the Fe ion inside the FeAs blocking unit is slightly reduced from +2.0 to  $+(2 - \delta)$ . Surprisingly, when the sample  $\text{Sr}_2\text{VO}_{2.5}\text{FeAs}$  is cooled down to the superconducting state, a structural reconstruction process occurs as is inferred from the *in situ* TEM cooling experiments. The evolution of superconductivity on oxygen stoichiometry can further be supported by the dependence of the Hall coefficient and resistivity. Our findings might shed new light on understanding the superconductivity of the  $\text{Sr}_2\text{VO}_{3-\delta}\text{FeAs}$  system.

DOI: [10.1103/PhysRevB.90.104503](https://doi.org/10.1103/PhysRevB.90.104503)

PACS number(s): 74.25.Dw, 74.25.nj, 74.70.Xa, 76.60.-k

## I. INTRODUCTION

The  $\text{Sr}_2\text{VO}_{3-\delta}\text{FeAs}$  superconductor with  $T_c$  at about 37.2 K was found in 2009 [1]. The unique feature of this oxyarsenide Fe-based superconductor lies in the fact that the occurrence of superconductivity depends essentially on the intrinsic oxygen deficiency rather than the extrinsic element dopant. Superconducting transition temperatures of  $\text{Sr}_2\text{VO}_{3-\delta}\text{FeAs}$  drop down monotonically with the increase of stoichiometry oxygen deficiency, in which the related mechanism has not been clarified yet. In order to understand this puzzling issue, significant research efforts have been devoted to understanding this novel superconductivity phenomenon [1–10].

Although many studies on  $\text{Sr}_2\text{VO}_{3-\delta}\text{FeAs}$  are available from literatures, many of them are not consistent with each other. A complex Fermi surface structure derived from vanadium electronic states was predicted from  $\text{Sr}_2\text{VO}_3\text{FeAs}$  by first-principles calculations [2].  $\text{Sr}_2\text{VO}_3$  blocks were calculated to be different metallic states: nonmagnetic, magnetic [3], and Mott-type magnetic states [4]. By combined techniques of x-ray absorption spectroscopy, Mossbauer spectrum, resistivity/magnetization measurement, self-doped, and a successive magnetic transition within the  $\text{VO}_2$  layer were found from  $\text{Sr}_2\text{VO}_3\text{FeAs}$  [5]. A small amount of vanadium doping and Fe/V mixing were found to suppress the superconductivity of  $\text{Sr}_2\text{VO}_3\text{FeAs}$ . The valence state of vanadium could be tuned between  $V^{1+}$  and  $V^{4+}$ , providing or accepting electron carriers from FeAs layers [7]. Very recently, via neutron scattering and density functional theory calculations, weak

magnetism and the Mott state of vanadium were found from the superconducting  $\text{Sr}_2\text{VO}_3\text{FeAs}$  [8]. The superconducting mechanisms might include oxygen deficiency and multiple valence of vanadium or iron [9–12]. Hence, there is no consensus on the evolution of superconductivity in  $\text{Sr}_2\text{VO}_{3-\delta}\text{FeAs}$  concerning the oxygen vacancies.

Most analysis seems to provide only indicative evidences but not exclusive ones. It is well known that the superconducting properties always exhibit strong dependence on the microstructure of Fe-based superconductors [13,14]. Microstructural study has been one of the most important approaches for superconductivity physics [15–18]. Until now, no detail microstructural investigation about the  $\text{Sr}_2\text{VO}_{3-\delta}\text{FeAs}$  superconductor has been reported, which is urgently needed.

Herein, by *in situ* TEM cooling observations combined TEM and EELS analyses with high-spatial resolution, oxygen vacancies inside the poor superconducting sample  $\text{Sr}_2\text{VO}_{2.5}\text{FeAs}$  were found to exhibit three different ways to balance this oxygen off-stoichiometry: (a) partial removal of SrO atom stripes; (b) periodic stacking faults; (c) slight Fe valence reduction. Comparatively, the superconducting sample  $\text{Sr}_2\text{VO}_{2.9}\text{FeAs}$  shows more perfect structure. Both microstructural features agree well with the dependency of the Hall effect and resistivity on temperature. All the findings might provide an important message to the understanding of the dependency of superconductivity property on its microstructural complexity features.

## II. RESULTS AND DISCUSSION

The  $\text{Sr}_2\text{VO}_{3-\delta}\text{FeAs}$  ( $\delta = 0.1, 0.5$ ) samples with layered structure feature (Figure S1) [19] were synthesized by

\*rcche@fudan.edu.cn

using a solid-state reaction method. A JEOL JEM-2100F (field-emission gun) transmission electron microscope (TEM) equipped with a post-column Gatan imaging filter (GIF-tridium) was used for TEM, STEM-HAADF, and EELS analyses. Acceleration voltage is 200 keV and HAADF point resolution can reach 0.11 nm with switching on an active vibration canceller mount (EM-Z06201 from Germany IDE Company). The thermal conductivity capability of  $\text{Sr}_2\text{VO}_{3-\delta}\text{FeAs}$  oxide is quite poor, easily accumulating thermal energy from the beam irradiation with 200 KeV primary energy and being heated. One big challenge that must be solved is that  $\text{Sr}_2\text{VO}_{3-\delta}\text{FeAs}$  is easily damaged under electron beam irradiation (200 KeV in TEM). To protect the beam-sensitive  $\text{Sr}_2\text{VO}_{3-\delta}\text{FeAs}$  structures, an *in situ* liquid-nitrogen TEM stage (Gatan-636 double-tilting holder) keeping at 255 K was used for all the TEM observations to minimize the beam damage. The main purpose to use *in situ* cooling TEM experiments is to study the structure transformation with temperature cooling down, three different cooling stages are used for various temperature ranges: Gatan-636 for RT–100 K, Gatan-HCHDT3010 for 20–100 K, and Gatan-ULTST for 10–20 K.

The energy resolution of EELS was  $\sim 0.70$  eV, as determined by the full width at half maximum (FWHM) of the zero-loss peak, so that fine structure fluctuation of white lines can be reflected. EELS data were recorded with a two-dimensional back-illuminated charge-coupled device camera (4000 2700 pixels) with a low read-out noise and a negligible dark count noise. To avoid electron channeling effects, the selected sample was tilted slightly off the zone axis by  $2^\circ$ – $4^\circ$ . The convergence angle was about 0.7 mrad ( $q \approx 0.04 \text{ \AA}^{-1}$ ) and the collection angle was  $\sim 3$  mrad ( $q \approx 0.17 \text{ \AA}^{-1}$ ). EELS data were acquired with a dispersion of 0.03 eV per channel for monitoring the fine structure change of white lines. High angle annular dark field imaging (HAADF) was carried out using the GATAN-777 package and the JEOL-STEM scanning system (ASID-2000). The spherical and chromatic aberration coefficients ( $C_s$  and  $C_c$ , respectively) of the objective lens were 0.5 and 1.1 mm, respectively. The annular dark-field detector for ADF-STEM ranged from 42 to 65 mrad. The digital micrograph software (GATAN) was used for image recording/processing. The dc susceptibility of the samples was measured on a superconducting quantum interference device (Quantum Design, magnetic property measurement system 7 T). The resistivity and Hall-effect measurements were done using a six-probe technique on this system with magnetic fields up to 9 T. The temperature stabilization was better than 0.1% and the resolution of the volt meter was better than 10 nV [9].

To unambiguously determine the crystal structural parameters of  $\text{Sr}_2\text{VO}_{3-\delta}\text{FeAs}$  ( $\delta = 0.1, 0.5$ ) superconductors, robust evidences including high-resolution TEM (HRTEM) images and electron diffraction (ED) patterns were obtained along the orientation of the [120] zone axis, respectively [Figs. 1(a)–1(d)]. As far as we know, this is the first report of electron microscopy observations for the microstructural study of  $\text{Sr}_2\text{VO}_{3-\delta}\text{FeAs}$ . Based on indexing the HRTEM and ED data, lattice parameters were determined to be  $a = 3.91 \text{ \AA}^{-1}$ ,  $c = 15.65 \text{ \AA}^{-1}$  for  $\text{Sr}_2\text{VO}_{2.9}\text{FeAs}$  and  $a = 3.98 \text{ \AA}^{-1}$ ,  $c = 15.72 \text{ \AA}^{-1}$  for  $\text{Sr}_2\text{VO}_{2.5}\text{FeAs}$ , respectively. The two vertical

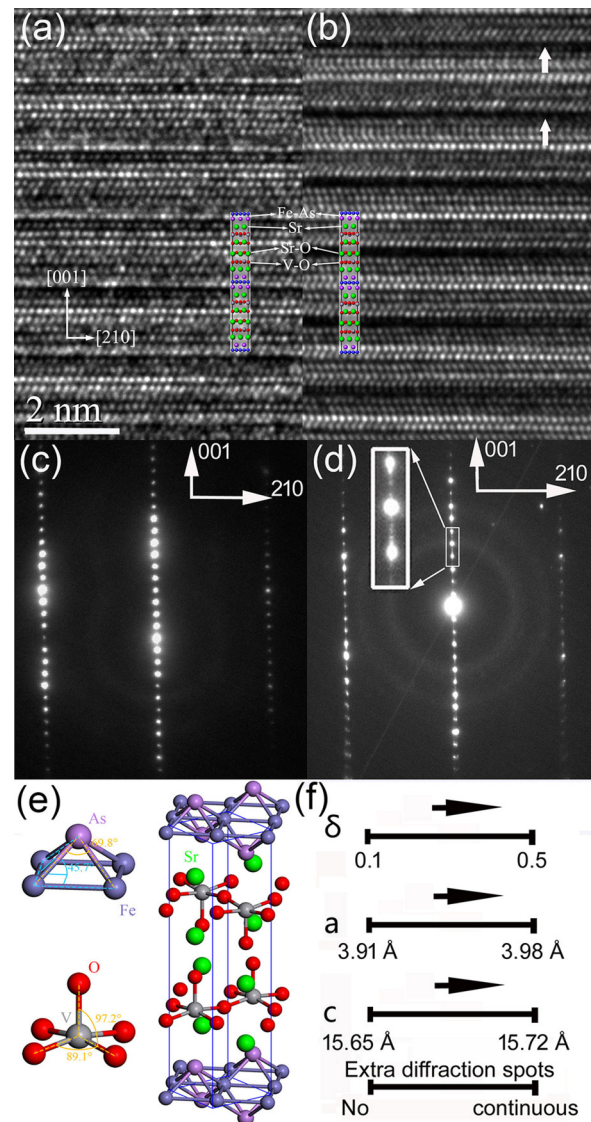


FIG. 1. (Color online) HRTEM images and electron diffraction patterns along the [120] zone axis of (a), (c)  $\text{Sr}_2\text{VO}_{2.9}\text{FeAs}$ , and (b) and (d)  $\text{Sr}_2\text{VO}_{2.5}\text{FeAs}$ . (e) Crystal model and bond parameters of  $\text{Sr}_2\text{VO}_{3-\delta}\text{FeAs}$  ( $\delta = 0.1, 0.5$ ). (f) Dependency of lattice parameters (a) and (c) and extra diffraction features of both samples on  $\delta$ .

sets of basic unit fringes could be well attributed to (001) and (210) crystal planes of  $P4/nmm$   $\text{Sr}_2\text{VO}_{3-\delta}\text{FeAs}$ . The positions of each type of atoms agree well with the  $\text{Sr}_2\text{VO}_{3-\delta}\text{FeAs}$  unit [Figs. 1(a), 1(b), and 1(e)]. Both phases consist of an alternative stacking of antiferroite  $\text{Fe}_2\text{As}_2$  layers and perovskite  $\text{Sr}_2\text{VO}_{3-\delta}$  blocks, respectively, serving as the superconductive electron layer and charge carrier reservoir.

Although the above crystal parameters are basically in agreement with the previous XRD measurements, comparative analysis of crystal structures between  $\text{Sr}_2\text{VO}_{3-\delta}\text{FeAs}$  ( $\delta = 0.1, 0.5$ ) shows evident differences induced by oxygen vacancy: (1) There was a slight lattice expansion of  $\sim 0.07 \text{ \AA}^{-1}$  found from both  $a$  and  $c$  length after 20% ( $\delta$  changing from 0.1 to 0.5) of stoichiometric oxygen vacancy was injected into the original  $\text{Sr}_2\text{VO}_3$  blocks; (2) unexpectedly, around the middle position

of each unit cell, a line of atom stripes with dark contrast running vertical to the [001] orientation could be periodically found from  $\text{Sr}_2\text{VO}_{2.5}\text{FeAs}$  instead of the  $\text{Sr}_2\text{VO}_{2.9}\text{FeAs}$  lattice [arrows of Fig. 1(b)]. The interval space between two dark lines is around one unit distance bridging two (001) planes; (3) extra diffraction spots with intermittent streak features could be clearly found between the dominant diffraction spots of  $\text{Sr}_2\text{VO}_{2.5}\text{FeAs}$  rather than that of  $\text{Sr}_2\text{VO}_{2.9}\text{FeAs}$ , indicating the occurrence of the abnormal stacking sequence of atom or cation layers distributed along the [001] orientation.

After indexing HRTEM images by using the lattice parameters of  $\text{Sr}_2\text{VO}_{3-\delta}\text{FeAs}$  [Fig. 1(e)], partially missing SrO atomic chains was supposed to be responsible for this periodical dark stripe contrast. To confirm this assumption, the specimen region with larger size was observed and the similar periodic weak contrast was statistically found, which exhibits the existence of the abnormal stacking sequences of atomic layers along the [001] orientation (TEM zoom-in image in Figure S2). The possible mechanism lies in the fact that off-stoichiometric oxygen of  $\delta = 0.5$  (20% vacancy) could affect its nearest neighbor bonding atoms such as Sr and V and lead to the formation of the SrO vacancy or VO vacancy to maintain electrically neutral of the whole  $\text{Sr}_2\text{VO}_{3-\delta}\text{FeAs}$  crystal. In our case, the partial absence of SrO stripes destroys the original perfect periodic structure, which might scatter the TEM beam to make rather weak TEM image contrast. It is reasonable to assume that through the static electric coupling mode, the superconducting property might be sensitively modulated by tuning the off-stoichiometry degree of oxygen ( $\delta$ ) and the formation of stacking faults [Figs. 1(b), 3, and 4(b)]. With  $\delta$  increasing from 0.1 to 0.5, this coupling effect becomes more evident according to layer-by-layer stacking sequence (along SrO-VO-FeAs) and the valence state change of metallic elements was speculated. To verify this assumption, EELS analysis was carried out, which can precisely provide valence information based on electron excitation from the spin-orbit split  $2p$  core hole to the  $3d$  empty states in the conduction bands during ionization transitions.

Both  $\text{Sr}_2\text{VO}_{3-\delta}\text{FeAs}$  ( $\delta = 0.1, 0.5$ ) superconductors contain V- $L_{2,3}$ , O-K, and Fe- $L_{2,3}$  at energy region of  $\sim 513$ ,  $\sim 532$ , and  $\sim 708$  eV, respectively (Fig. 2). In particular, both  $\text{Sr}_2\text{VO}_{2.9}\text{FeAs}$  and  $\text{Sr}_2\text{VO}_{2.5}\text{FeAs}$  display a pair of intense Fe- $L_{2,3}$  edges, the so-called white lines, whose tiny fluctuation of positions, intensities, and fine shapes reflect accurately the valence state and atomic site coordination of iron and vanadium. The Fe- $L_3$  edge of  $\text{Sr}_2\text{VO}_{2.9}\text{FeAs}$  shifts  $\sim 0.9$  eV to the right direction compared to that of  $\text{Sr}_2\text{VO}_{2.5}\text{FeAs}$ , indicating that the oxidized degree by its environment becomes weaker than that of  $\text{Sr}_2\text{VO}_{2.5}\text{FeAs}$ . To quantitatively identify the valence state of the Fe ion, the  $L^3/L^2$  integral ratio computed from relative area proportions covered by Fe- $L_{2,3}$  edges extracted from EELS data were computed for  $\text{Sr}_2\text{VO}_{3-\delta}\text{FeAs}$  ( $\delta = 0.1, 0.5$ ) according to the previous well-established method [20–22]. A valence state reduction from  $+2.0$  to  $+(2 - \delta)$  was determined while  $\delta$  changes from 0.1 to 0.5, where  $\delta$  is less than 0.2. In order to statistically confirm this subtle valence change of Fe, x-ray photoelectron spectroscopy (XPS) analysis was carried out, revealing again the slight valence reduction (Figure S3).

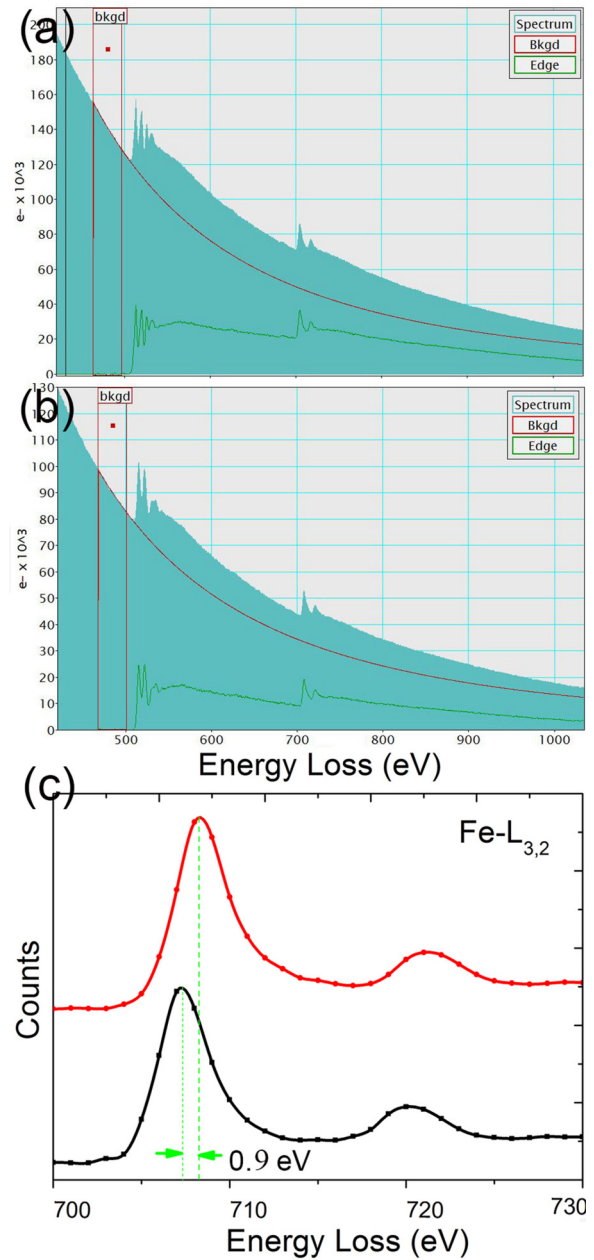


FIG. 2. (Color online) EELS of (a)  $\text{Sr}_2\text{VO}_{2.9}\text{FeAs}$  and (b)  $\text{Sr}_2\text{VO}_{2.5}\text{FeAs}$  including raw data and background-subtracted data, with V- $L_{2,3}$  at energy region 513 eV, O-K at 532 eV, and Fe- $L_{2,3}$  at 708 eV. (c) White lines of Fe- $L_{2,3}$  of both samples.

The oxygen deficiency introduced into  $\text{Sr}_2\text{VO}_3\text{FeAs}$  was realized by weighting according to the stoichiometry ratio of  $\text{Sr}_2\text{VO}_{3-\delta}\text{FeAs}$  and subsequent homogeneous mixing ( $\delta = 0.1, 0.5$ ) before calcination. According to the unique layered-structural feature of  $\text{Sr}_2\text{VO}_{3-\delta}\text{FeAs}$  crystal, oxygen deficiency should be doped into the  $\text{Sr}_2\text{VO}_{3-\delta}$  block instead of the FeAs block. Before doping, the original valence state of Sr, V, O, Fe, and As should be the standard value of  $+2$ ,  $+3$ ,  $-2$ ,  $+2$ , and  $-3$ , respectively, leading to a  $+1$  valence for the  $\text{Sr}_2\text{VO}_3$  block and  $-1$  valence for the FeAs block. After 20% oxygen vacancy was introduced into the  $\text{Sr}_2\text{VO}_3$  block, the valence state of the  $\text{Sr}_2\text{VO}_{3-\delta}$  block becomes a little higher than the standard

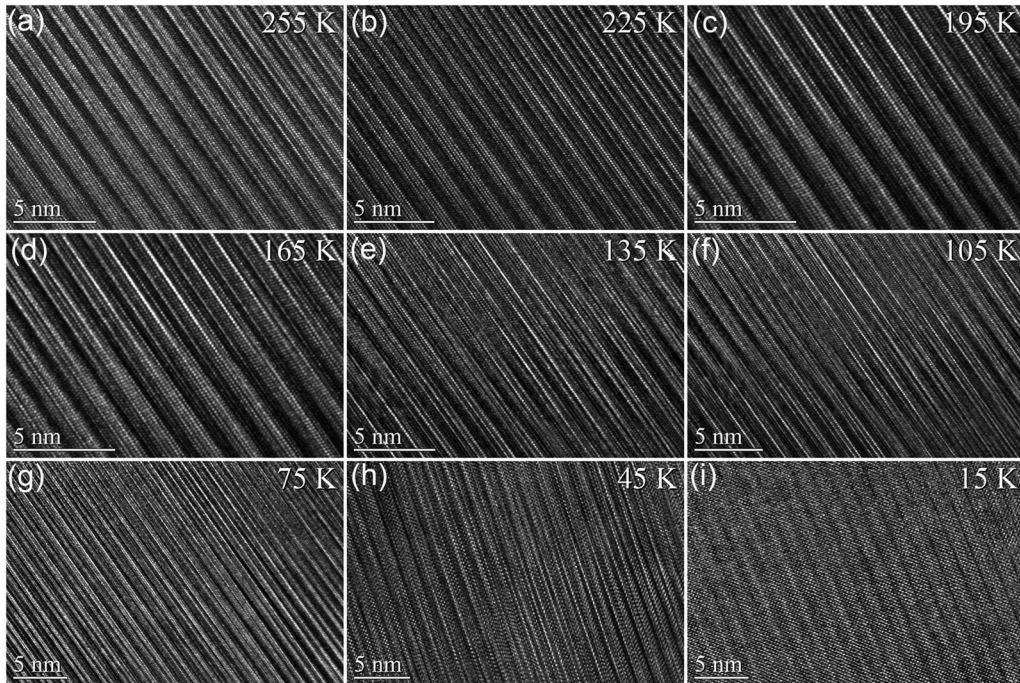


FIG. 3. Structural evolution with the temperature cooling down from 255 to 15 K via *in situ* TEM cooling experiments. Three different cooling stages are used for various temperature ranges: Gatan-636 for RT–100 K, Gatan-HCHDT3010 for 20–100 K, and Gatan-ULTST for 10–20 K.

+1 valence. The valence state of Fe was obliged to deviate from the standard value and reduce to be about (2−) under the constraint coupling between the positive FeAs and negative  $\text{Sr}_2\text{VO}_{3-\delta}$  block inside the whole  $\text{Sr}_2\text{VO}_{3-\delta}\text{FeAs}$  structure to remain electrically neutral. Moreover, the fine structure difference between the oxygen K edges of the  $\text{Sr}_2\text{VO}_{3-\delta}\text{FeAs}$  ( $\delta = 0.1, 0.5$ ) superconductors is evident. Two distinct sharp peaks (a and b) can be found from the O 1s core-loss spectra of  $\text{Sr}_2\text{VO}_{2.9}\text{FeAs}$ . Peak a and b correspond to the transition from the O 1s states towards the hybrid states composed of metallic element electrons and the O 2p joint vacant states [20]. However, in the case of the poor superconductor  $\text{Sr}_2\text{VO}_{2.5}\text{FeAs}$ , peak b ( $\sim 532.0$  eV) was transformed into one bump shoulder, indicating the variations of hybridized electron states made up of O, Sr, and V, which was induced by oxygen vacancy injection. Neither evident energy shift nor the ratio change of the integral area covered by the  $V-L_{2,3}$  edges can be found, indicating that oxygen vacancy injection might not induce the valance variation of the V element. To accurately discriminate the valance value of V is rather difficult because that the excitation energy edges of  $V-L_{2,3}$  (513 eV) and O-K (530 eV) overlap closely. It should be mentioned that at least 20 individual regions are selected for EELS examination during our experiment to provide consistent data with statistical reliability.

Even though the distance between FeAs layers within one  $\text{Sr}_2\text{VO}_{3-\delta}\text{FeAs}$  unit is quite large ( $\sim 1.6$  nm) for Cooper electron pair coupling between two FeAs superconducting layers (top/bottom of one unit), the above experimental facts confirm that the static electric coupling can be effectively enhanced between the charge carrier reservoir and superconductive electron blocks via the introduction of oxygen vacancy.

Therefore, through the strategy of tuning oxygen deficiency carriers,  $\text{Sr}_2\text{VO}_{3-\delta}\text{FeAs}$  becomes a platform for static electric coupling, which leads to the adjustment of antiferromagnetism and superconductivity.

The structural features in  $\text{Sr}_2\text{VO}_{2.5}\text{FeAs}$  were characterized by *in situ* cooling TEM observations along the [120] crystallographic direction from 255 K (nonsuperconducting state) down to 15 K (superconducting state). Figures 3(a)–3(i) shows a series of HRTEM images obtained at different temperatures, revealing notable microstructural alterations of stripelike lamellae. Typically, the width of the SrO atom stripes with dark contrast becomes smaller with the temperature cooling down and finally invisible at 15 K (white lines in Fig. 3). Our experimental results suggest that the superconducting property associated with microstructure in this oxygen-deficient system depend considerably on temperature. This is a striking result which indicates a subtle evolution of the microstructure when the system enters into the superconducting state. This correlation may be induced by the inevitable connection between the electron pairing on the FeAs4 layer and the possible magnetism on the  $\text{Sr}_2\text{VO}_{3-\delta}$  layer [5]. It remains to get a thorough understanding of this phenomenon.

Careful HRTEM observation reveals that different types of crystal defects exist inside  $\text{Sr}_2\text{VO}_{2.9}\text{FeAs}$  and  $\text{Sr}_2\text{VO}_{2.5}\text{FeAs}$  [Figs. 4(a) and 4(b)]. Only a small concentration of point vacancies randomly distributed inside the  $\text{Sr}_2\text{VO}_{2.9}\text{FeAs}$  matrix could be found, which might facilitate the coupling between  $\text{Sr}_2\text{VO}_{3-\delta}$  and FeAs blocks [circles in Fig. 4(a)]. On the contrary, high density of stacking faults (SF) parallel to the [001] direction could be readily found from  $\text{Sr}_2\text{VO}_{2.5}\text{FeAs}$  rather than  $\text{Sr}_2\text{VO}_{2.9}\text{FeAs}$ . Hence, certain

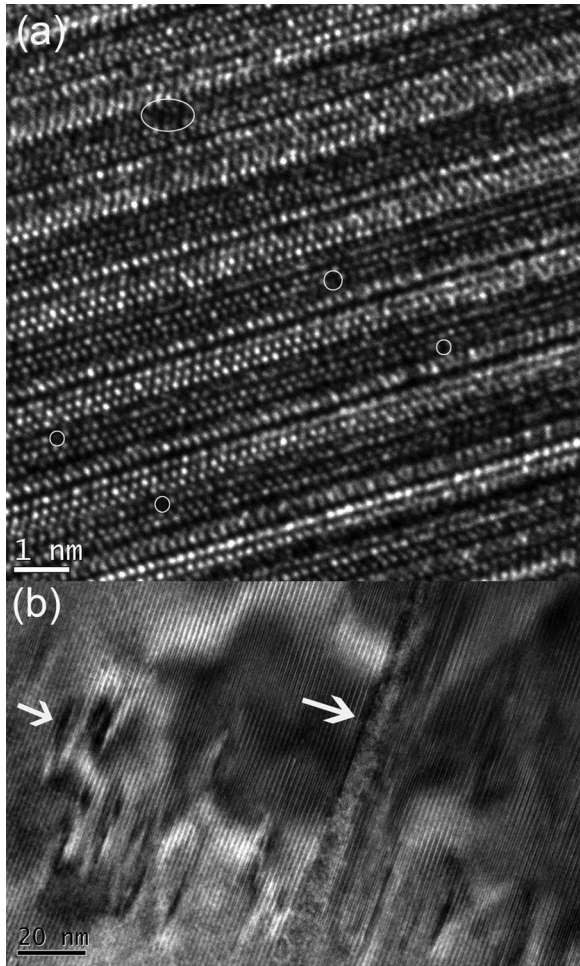


FIG. 4. (a) Microstructure of  $\text{Sr}_2\text{VO}_{2.9}\text{FeAs}$  with limited density of cation point vacancy. (b) Stacking faults of  $\text{Sr}_2\text{VO}_{2.5}\text{FeAs}$ .

stacking deviation occurred inside the original stacking sequence of  $\dots(\text{FeAs} \cdot \text{SrVO} \cdot \text{FeAsSrVO})_n\dots$ , forming a blocking effect of superconducting electrons along the  $c$  axis.

The temperature dependence of resistivity normalized to 300 K is shown in Fig. 5(a) for samples  $\delta = 0.1$  (optimally doped) and  $\delta = 0.5$  (oxygen deficient). Since the resistivity can be written as  $\rho = \rho_0 + m^*/(n\tau e^2)$ , the residual resistivity of  $\text{Sr}_2\text{VO}_{3-\delta}\text{FeAs}$  is very small for the sample  $\delta = 0.1$ , indicating good metallic behavior. For the oxygen deficient sample with  $\delta = 0.5$ , the normalized residual resistivity is much enhanced suggesting a strong impurity scattering effect in the oxygen-deficient sample. The Hall coefficient was measured and determined through  $dV_{\text{Hall}}/dH$  at fixed temperatures and shown in Fig. 5(b). The lower values of the Hall coefficient RH in the sample  $\delta = 0.5$  indicate a higher electron doping in this sample compared with that of  $\delta = 0.1$ . The strong scattering effect in the sample  $\delta = 0.5$  could be interpreted by the disordered atomic lattice of both the SF structure and cation vacancy seen by the above microstructure analysis. The oxygen vacancies, stripe structure with dark contrast, and even high density of SFs destroy the original perfect crystal structure of  $\text{Sr}_2\text{VO}_{2.9}\text{FeAs}$ , thus forming a barrier at cell interfaces and blocking the motion of superconducting

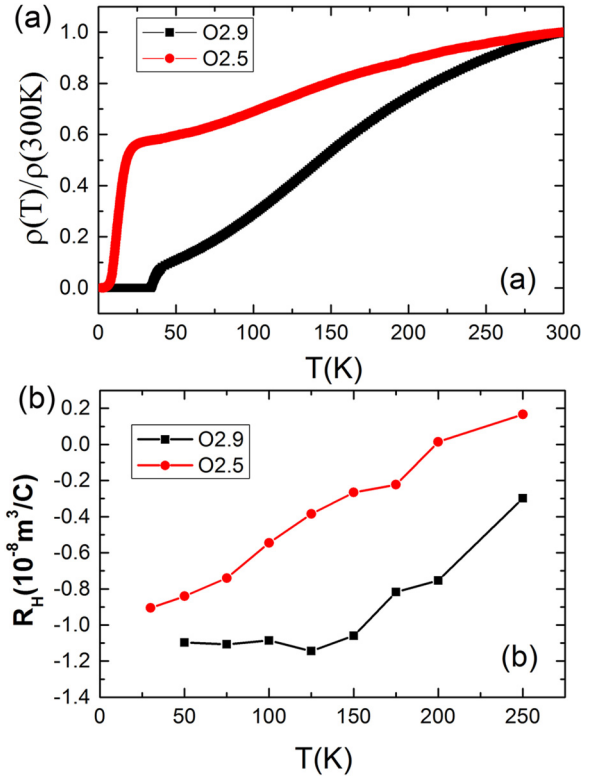


FIG. 5. (Color online) (a) Temperature dependence of the normalized resistivity of the samples  $\text{Sr}_2\text{VO}_{3-\delta}\text{FeAs}$  with  $\delta = 0.1$  (square) and 2.5 (circles). (b) Temperature dependence of the Hall coefficient RH measured at a magnetic field of 9 T.

electrons along the  $c$  axis, which is crucially responsible for the degradation of superconducting transition temperature. Both the electric transport data and the TEM measurements indicate enhanced impurity scattering which could be induced by the nonmagnetic oxygen vacancies, or stacking faults in the poor superconducting sample  $\text{Sr}_2\text{VO}_{2.9}\text{FeAs}$ . This is consistent with the expectation of a the  $S_{\pm}$  pairing model [23,24].

### III. SUMMARY

In summary, structural investigations by means of the *in situ* TEM ultrahigh resolution cooling experiment on the poor superconducting  $\text{Sr}_2\text{VO}_{2.5}\text{FeAs}$  sample reveal that oxygen vacancy induces stacking faults, Fe valence reduction, and SrO atom stripe extraction. While the superconducting  $\text{Sr}_2\text{VO}_{2.9}\text{FeAs}$  sample shows a much better structure with only a limited amount of point vacancies, TEM analysis reveals that oxygen vacancy sensitively modifies the original stacking structure. The Hall effect and resistivity measurements were consistent with microstructural evidences in terms of the influence on the evolution of superconductivity. Our results suggest that an enhanced scattering due to oxygen vacancies, the stacking faults, and lowered valence of the Fe irons are harmful to superconductivity, which is consistent with the exception of the  $S_{\pm}$  pairing model. Our results might provide an in-depth understanding of the evolution of superconductivity in the  $\text{Sr}_2\text{VO}_{3-\delta}\text{FeAs}$  system.

## ACKNOWLEDGMENTS

This work was supported by the National Natural Foundation of China (Grants No. 51102050, No. 51172047, and No. 11274066) and the Ministry of Science and Technology of China (973 Projects No.

2013CB932901, No. 2011CBA00102, No. 2012CB821403, and No. 2009CB930803). This project was sponsored by Shanghai Pujiang Program and “Shu Guang” project of Shanghai Municipal Education Commission and Shanghai Education Development Foundation (09SG01).

- 
- [1] X. Zhu, F. Han, G. Mu, P. Cheng, B. Shen, B. Zeng, and H.-H. Wen, *Phys. Rev. B* **79**, 220512 (2009).
- [2] I. I. Mazin, *Phys. Rev. B* **81**, 020507 (2010).
- [3] K. Ueshima, F. Han, X. Zhu, H.-H. Wen, S. Kawasaki, and G.-q. Zheng, *Phys. Rev. B* **89**, 184506 (2014).
- [4] H. Nakamura and M. Machida, *Phys. Rev. B* **82**, 094503 (2010).
- [5] A. S. Sefat, D. J. Singh, V. O. Garlea, Y. L. Zuev, M. A. McGuire, and B. C. Sales, *Physica C* **471**, 143 (2011).
- [6] G.-H. Cao, Z. Ma, C. Wang, Y. Sun, J. Bao, S. Jiang, Y. Luo, C. Feng, Y. Zhou, Z. Xie, F. Hu, S. Wei, I. Nowik, I. Felner, L. Zhang, Z. Xu, and F.-C. Zhang, *Phys. Rev. B* **82**, 104518 (2010).
- [7] M. Tegel, T. Schmid, T. Stürzer, M. Egawa, Y. Su, A. Senyshyn, and D. Johrendt, *Phys. Rev. B* **82**, 140507 (2010).
- [8] F. Hummel, Y. Su, A. Senyshyn, and D. Johrendt, *Phys. Rev. B* **88**, 144517 (2013).
- [9] H.-H. Wen, X. Zhu, F. Han, G. Mu, P. Cheng, B. Shen, and B. Zeng, *Physica C* **470** (Suppl. 1), S263 (2010).
- [10] R. Che, R. Xiao, C. Liang, H. Yang, C. Ma, H. Shi, and J. Li, *Phys. Rev. B* **77**, 184518 (2008).
- [11] T. Katagiri and T. Sasagawa, *Physica C* **484**, 16 (2013).
- [12] B. Rosenstein, I. Shapiro, and B. Y. Shapiro, *Physica C* **102**, 57002 (2013).
- [13] Y. Xu, M. Suenaga, J. Taftø, R. L. Sabatini, A. R. Moodenbaugh, and P. Zolliker, *Phys. Rev. B* **39**, 6667 (1989).
- [14] Y. Li, E. Baggio-Saitovitch, Y. B. Wang, G. H. Cao, N. Chen, Z. X. Zhao, and L. Wei, *Physica C* **315**, 129 (1999).
- [15] S. Avci, J. M. Allred, O. Chmaissem, D. Y. Chung, S. Rosenkranz, J. A. Schlueter, H. Claus, A. Daoud-Aladine, D. D. Khalyavin, P. Manuel, A. Llobet, M. R. Suchomel, M. G. Kanatzidis, and R. Osborn, *Phys. Rev. B* **88**, 094510 (2013).
- [16] Y.-L. Sun, H. Jiang, H.-F. Zhai, J.-K. Bao, W.-H. Jiao, Q. Tao, C.-Y. Shen, Y.-W. Zeng, Z.-A. Xu, and G.-H. Cao, *J. Am. Chem. Soc.* **134**, 12893 (2012).
- [17] S. Singh, J. Shimoyama, A. Yamamoto, H. Ogino, and K. Kishio, *Physica C: Superconductivity* **494**, 57 (2013).
- [18] R. M. Fernandes, A. E. Böhmer, C. Meingast, and J. Schmalian, *Phys. Rev. Lett.* **111**, 137001 (2013).
- [19] See Supplemental Material at <http://link.aps.org/supplemental/10.1103/PhysRevB.90.104503> for details of the TEM images and EELS experiments.
- [20] R. Che, R. Xiao, C. Liang, H. Yang, C. Ma, H. Shi, and J. Li, *Phys. Rev. B* **77**, 184518 (2008).
- [21] X. Guo, M. Wang, X. Huang, P. Zhao, X. Liu, and R. Che, *J. Mater. Chem. A* **1**, 8775 (2013).
- [22] X. Huang, M. Wang, and R. Che, *J. Mater. Chem. A* **2**, 9656 (2014).
- [23] I. I. Mazin, D. J. Singh, M. D. Johannes, and M. H. Du, *Phys. Rev. Lett.* **101**, 057003 (2008).
- [24] K. Kuroki, S. Onari, R. Arita, H. Usui, Y. Tanaka, H. Kontani, and H. Aoki, *Phys. Rev. Lett.* **101**, 087004 (2008).